Journal of Applied Physics ARTICLE scitation.org/journal/jap

Defect suppression in wet-treated etched-and-regrown nonpolar *m*-plane GaN vertical Schottky diodes: A deep-level optical spectroscopy analysis

Cite as: J. Appl. Phys. **128**, 185703 (2020); doi: 10.1063/5.0018829
Submitted: 17 June 2020 · Accepted: 29 October 2020 ·
Published Online: 12 November 2020

Andrew Aragon,[1,a)] Morteza Monavarian,[1] Greg Pickrell,[2] Mary Crawford,[2] Andrew Allerman,[2] Daniel Feezell,[1] and Andrew M. Armstrong[2]

AFFILIATIONS

[1]Center for High-Technology Materials, The University of New Mexico, Albuquerque, New Mexico 87106, USA
[2]Sandia National Laboratories, Albuquerque, New Mexico 87123, USA

[a)]**Author to whom correspondence should be addressed:** aragon63@unm.edu

ABSTRACT

Steady-state photocapacitance (SSPC) was conducted on nonpolar *m*-plane GaN *n*-type Schottky diodes to evaluate the defects induced by inductively coupled plasma (ICP) dry etching in etched-and-regrown unipolar structures. An ∼10× increase in the near-midgap E_c – 1.9 eV level compared to an as-grown material was observed. Defect levels associated with regrowth without an etch were also investigated. The defects in the regrown structure (without an etch) are highly spatially localized to the regrowth interface. Subsequently, by depth profiling an etched-and-regrown sample, we show that the intensities of the defect-related SSPC features associated with dry etching depend strongly on the depth away from the regrowth interface, which is also reported previously [Nedy *et al.*, Semicond. Sci. Technol. **30**, 085019 (2015); Fang *et al.*, Jpn. J. Appl. Phys. **42**, 4207–4212 (2003); and Cao *et al.*, IEEE Trans. Electron Devices **47**, 1320–1324 (2000)]. A photoelectrochemical etching (PEC) method and a wet AZ400K treatment are also introduced to reduce the etch-induced deep levels. A significant reduction in the density of deep levels is observed in the sample that was treated with PEC etching after dry etching and prior to regrowth. An ∼2× reduction in the density of E_c – 1.9 eV level compared to a reference etched-and-regrown structure was observed upon the application of PEC etching treatment prior to the regrowth. The PEC etching method is promising for reducing defects in selective-area doping for vertical power switching structures with complex geometries [Meyers *et al.*, J. Electron. Mater. **49**, 3481–3489 (2020)].

INTRODUCTION

GaN-based vertical power electronic structures have gained tremendous attention due to their wide material bandgap, high electron saturation velocity, and high thermal conductivity.[5–7] Many complex vertical structure designs require selective-area-doping via etching and regrowth of *n*- and/or *p*-type GaN, which makes the design technologically more complicated compared to, for instance, elemental semiconductors such as Si, in which ion implantation can easily be done.[8,9] The study of etched-and-regrown surfaces on GaN-based materials is thus technologically relevant due to the growth and fabrication requirements for emerging vertical power electronic devices with complex geometries such as junction gate field-effect transistors (JFETs) and current aperture vertical electron transistors (CAVETs).[10,11] The vertical geometry has significant advantages over lateral designs such as smaller form factor, reduced current crowding, scalable blocking voltage without increasing on-resistance significantly, and increased field management.[12–18] Most previous works on vertical power devices has concentrated on the basal *c*-plane orientation.[19,20] However, numerous etched-and-regrown vertical device designs contain junction areas incorporating planes other than the *c*-plane, such as the nonpolar *m*-plane or *a*-plane. Therefore, it is expected that deep-level defects generated during dry etching and/or regrowth processes occur on both the *c*-plane bottom and *m*-plane sidewalls. Hence, the investigation of deep-level defects on the nonpolar *m*-plane is important for understanding defect-related and damage-induced current leakage mechanisms in etched-and-regrown diodes.

Here, we investigate regrown and etched-and-regrown *m*-plane GaN vertical Schottky diodes by steady-state photocapacitance (SSPC) by comparing changes in the defect concentration relative to a continuously grown film. Elevated defect concentrations were localized at regrowth interfaces even without a plasma etch. Regrowth on plasma-etched surfaces produced even higher peak defect concentrations near the regrowth interface, and elevated defectivity propagated into the regrown region. Post-etch surface treatment using AZ400K prior to regrowth reduced the defect concentration at the regrown interface. We also introduced a photoelectrochemical (PEC) wet etch treatment to remove dry-etch-induced damage at the regrowth interface of the etched-and-regrown diodes. The effectiveness of the PEC etch treatment in reducing the dry-etch-induced damage near the regrowth interface was also investigated and compared with AZ400K. The concentration of the near-midbandgap defect level trended with reverse leakage, suggesting that this defect is a major contributor to diode leakage.

EXPERIMENTAL DETAILS

GaN Schottky diode structures were grown using a Veeco metal-organic chemical vapor deposition (MOCVD) system on a freestanding *m*-plane GaN substrate with a −0.95° mis-cut toward the minus *c*-direction from Mitsubishi Chemical Corporation (MCC). The substrate is *n*-type Si doped ($n_0 = 1 \times 10^{17}$ cm^{-3}). The small crystal off-angle minimizes the roughness of the overgrown GaN epilayer by mitigating pyramidal hillocks.[21] The epitaxial layers were grown at a pressure of 500 Torr using trimethylgallium (TMGa) and ammonia (NH_3) as precursors for elemental Ga and N, respectively. The *n*-type dopant is introduced using SiH_4 diluted in nitrogen. The *n*-GaN layers are grown at a substrate temperature of ∼960 °C measured by a pyrometer. The epitaxial growth consists of a 2-μm-thick *n*-type GaN buffer layer ([Si]: 6×10^{17} cm^{-3}) followed by a 250-nm-thick n^+-GaN ([Si]: $\sim 5 \times 10^{18}$ cm^{-3}) and a subsequent 5-μm-thick lightly doped *n*-type GaN (with $N_D - N_A$: $\sim 6 \times 10^{16}$ cm^{-3}) to serve as a drift region. The net doping concentration ($N_D - N_A$) of the lightly doped *n*-GaN drift layer was found using a capacitance–voltage (*C*–*V*) evaluation on a separate calibration sample. A schematic of the Schottky diode structure is shown in Fig. 1(a).

A total of five samples with various treatments at the regrowth interface were studied. Sample 1 (reference sample) was continuously grown without any interruption, etching, or surface treatment to serve as a reference baseline as-grown material for comparison. Sample 2 contained a regrowth interface without etching but with a solvent cleaning acetone/isopropanol/de-ionized water (Ace/IPA/DI) to intentionally introduce impurities at the regrowth interface. We note that interfacial impurities such as Si, O, and C are known to affect the reverse and off-state forward leakage current as well as reverse blocking voltage of vertical *p*–*n* diodes.[22] Sample 3 was regrown after 400 nm of dry etching using a PlasmaTherm Apex SLR inductively coupled plasma (ICP) etcher, in which $Cl/Ar/BCl_3$ at a chamber pressure of 5 mTorr with an ICP power of 130 W and a RF power of 30 W were used. Sample 4 was ICP etched using the same conditions as those for sample 3 but with a subsequent AZ400K treatment at 80 °C for 10 min prior to the regrowth. Sample 5 was also ICP etched (using the same conditions as those for samples 3 and 4) followed by a subsequent PEC etch (with an etch depth of 200 nm) in a 0.01M KOH in DI at room temperature with a mercury arc lamp positioned to have a surface flux of 100 mW/cm^2. The samples in this study were not exposed to any acid treatments as we have observed that doing so has yielded higher impurity incorporation with an increase in Si ($\sim 5 \times 10^{18}$ cm^{-3}), O ($\sim 2 \times 10^{18}$ cm^{-3}), and C ($\sim 2 \times 10^{18}$ cm^{-3}) at the regrown interface.[22] Table I summarizes all samples studied in this investigation along with the deep-level defect density results, which will be elaborated in the subsequent sections. Atomic force microscopy (AFM) root-mean-square (RMS) surface roughness scans ($20 \times 20\,\mu$m^2) are shown in Figs. 2(a)–2(d) of similarly grown m-plane GaN epilayers after the aforementioned surface treatments. Above 1 nm, surface roughness is attributed to ∼7.25 μm of GaN constituting the underlying *n*-type GaN buffer, n^{++}-GaN layer, and *n*-type GaN drift regions. Also, variations in roughness are ascribed to the differing treatments. A 250–500 nm *n*-type GaN ($n \sim 6 \times 10^{16}$ cm^{-3}) layer was regrown on samples 2–5 following surface treatments. AFM surface roughness scans ($20 \times 20\,\mu$m^2) of all samples are shown in Figs. 2(e)–2(i) prior to regrowth. The morphologies are similar to the previous surfaces before regrowth with a slight increase in roughness due to regrowth. All samples were processed into Schottky diode test devices for SSPC analysis.

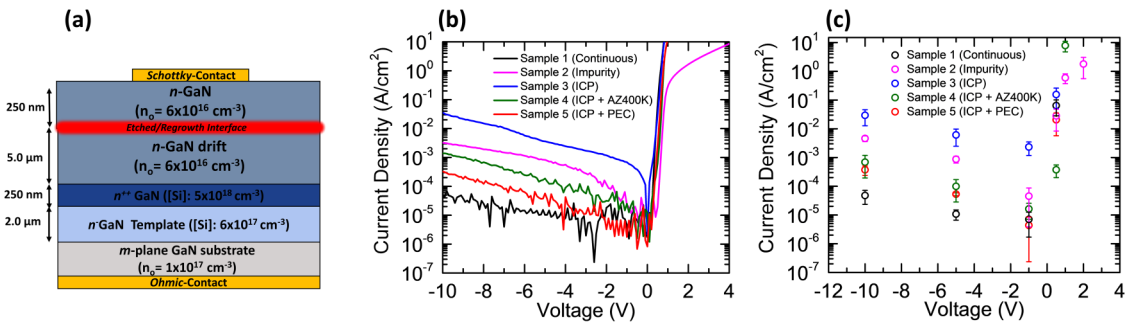

FIG. 1. (a) Schematic of Schottky diodes used in this study. (b) *J*–*V* characteristics of selected representative Schottky diodes from each sample. (c) *J*–*V* mean and standard deviation of statistical data.

Semi-transparent Ni contacts with 9 nm thickness were deposited on the top side to serve as Schottky contacts followed by a backside ohmic contact consisting of Ti/Al/Ni/Au (20/10/50/300 nm).

The current density–voltage (J–V) characteristics of a single representative diode out of ~10 measured diodes on each wafer are shown in Fig. 1(b). Statistical mean and standard deviation of ~10 measured diodes on each sample are shown in Fig. 1(c) at specific reverse and forward voltages of interest. According to the J–V results of Fig. 1(b), sample 1 shows the lowest reverse leakage current of $\sim 4 \times 10^{-5}$ A/cm^2 at −10 V among all the samples tested and a turn-on voltage of 0.7 V. A comparison of J–V data between the continuously grown (sample 1) and the regrown (sample 2) diodes indicates the influence of a regrowth process (without an etch) on current leakage. Sample 2 shows an ~100× larger reverse J compared to that of the reference (sample 1) ($\sim 3 \times 10^{-3}$ A/cm^2 compared to $\sim 4 \times 10^{-5}$ A/cm^2 at −10 V). A comparison of sample 3 shows the highest reverse leakage of $\sim 3 \times 10^{-2}$ A/cm^2 at −10 V of all samples with ~1000× increase in the reverse leakage compared to the reference (sample 1). The forward turn-on voltage of sample 3, however, is similar to that of the reference (sample 1) (0.7 V), indicating that dry-etch-induced damage has a more prominent effect on the reverse characteristics than on the forward characteristics of the Schottky diodes. An additional testing of AZ400K wet-treated ICP etched and regrown diodes (sample 4) shows a reduction in the reverse J ($\sim 1 \times 10^{-3}$ A/cm^2) compared to the ICP etched and regrown diodes (sample 3). Therefore, the removal of ICP etched damage regions using AZ400K shows a slight improvement in the reverse blocking voltage. Further comparison of an ICP etched (sample 3) and subsequent PEC etched (sample 5) diode shows further reduction of the reverse J ($\sim 3 \times 10^{-4}$ A/cm^2). The decrease in the reverse leakage current of sample 5 is attributed to the removal of the dry-etch-induced damage using PEC and shows that PEC was more effective at reducing the reverse leakage current than by AZ400K. The forward turn-on voltage is similar (0.7–0.8 V) for all samples. However, sample 2 exhibits a higher R_{on} than the rest of the samples. From our previous work, we expect the highest concentration of interfacial impurities ($>1 \times 10^{18}$ cm^{-3}) at the regrown interface.[22] Complete ionization has not been confirmed, but the higher R_{on} may be attributed to impurity compensation which may affect R_{on}. The elevation in deep levels may also indicate other phenomenon such as increased recombination or trapping at the regrown junction which may also lead to higher R_{on}, but further investigation is on-going.

Steady-state photocapacitance[23] (SSPC) was used to examine the type of deep level defects and lighted capacitance–voltage (LCV)[23] was used to measure the depth profile of defect concentrations in the regrown diodes. SSPC uses monochromatic, sub-bandgap-energy light to stimulate photoemission of carriers trapped at defect states in the depletion region of a diode. Upon photoemission, the carrier is swept out of the junction, and the remnant excess space-charge causes the depletion region to contract. The additional depletion capacitance is measured as a photocapacitance ΔC. When the energy of the mono-chromatic light becomes large enough to resonate with a deep level, thresholds appear in the SSPC spectrum at approximately E_o–d_{FC}, where E_o is the optical energy of the defect and d_{FC} is the Franck–Condon energy. The photon energy at which these thresholds occur is a hallmark of a defect. The saturation of the SSPC signal occurs at the bandgap energy. For the case of uniform doping, SSPC can quantify the deep level defect concentration (N_t). However, it was found in this study that the regrowth interface often was accompanied by a large spike in the doping. This rapidly varying doping concentration made conventional SSPC near the regrowth interfaces difficult from the standpoint of establishing N_t. Therefore, SSPC data are shown in as $\Delta C/C_0$ to focus only on defect energy thresholds.

Defect concentration was measured using LCV. LCV measures the depth profile of a defect's concentration by measuring the increase in the apparent doping concentration when the deep level defect is photo-ionized by continuous wave (CW) monochromatic illumination. A photon energy is chosen to cause photoemission of the defect with the lowest E_o, and the increase in the space-charge profile relative to that in the dark with all deep levels filled gives the N_t depth profile of that defect state. The extent of the measured depth profiles of capacitance–voltage (CV) and lighted capacitance–voltage (LCV) were determined largely by the existence of (or lack of) a UID doping spike at the regrown interface. For the regrown samples without PEC etch, the large UID doping spike at the regrowth interface restricted the depletion region and, therefore, CV and LCV sensitivity to near the regrowth interface. For the regrown sample with the PEC etch, the UID doping spike was not evident, and this allowed the depletion region to move much deeper into the sample. For the case of multiple defect states, the measurement is repeated with successively larger photon energies chosen to optically excite defects one at a time.

SSPC and LCV measurements were performed at room temperature using a Xe arc lamp source filtered through a ¼ meter

TABLE I. Summarized deep-level defect density results for all the samples investigated.

Sample No.	Surface treatment	Above regrown interface			Near regrown interface		
		E_c − 1.9 eV (×10^{14} cm^{-3})	(E_c − 2.9 eV) (×10^{14} cm^{-3})	(E_c − 3.3 eV) (×10^{14} cm^{-3})	(E_c − 1.9 eV) (×10^{14} cm^{-3})	(E_c − 2.9 eV) (×10^{14} cm^{-3})	(E_c − 3.3 eV) (×10^{14} cm^{-3})
1	N/A	1	30	70	N/A	N/A	N/A
2	Ace/IPA/DI	2	20	30	2 000	1600	3 300
3	ICP (400 nm)	10	200	1000	85 600	5030	81 600
4	ICP (400 nm) + AZ400K	1	30	30	300	300	800
5	ICP (400 nm) + PEC (200 nm)	4	90	30	30	50	70

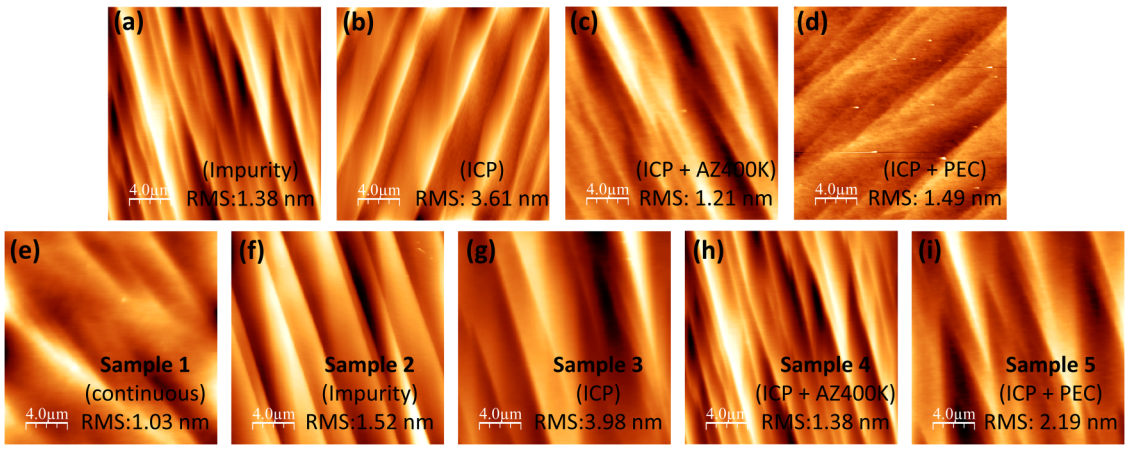

FIG. 2. AFM images of the *m*-plane GaN surface after 7.25 μm of growth and subsequent (a) impurity treatment, (b) ICP etch, (c) ICP etch and AZ400K treatment, (d) ICP etch and PEC etch. AFM images before processing of, (e) sample 1 continuous growth, (f) sample 2 impurity + regrowth, (g) sample 3 ICP etch + regrowth, (h) sample 4 ICP etch + AZ400K treatment + regrowth, (i) sample 5 ICP etch + PEC etch + regrowth.

monochromator with mode-sorting filters to achieve monochromatic illumination from 1.20 to 3.50 eV at a photon flux of 5×10^{16} cm^{-2} s^{-1}. A collimating lens and a focusing lens were used to image the beam on the diode's semi-transparent Schottky contact. For SSPC, a measurement and fill pulse bias of 0 and +0.5 V were used, respectively. LCV and SSPC measurements were taken at 1 MHz.

RESULTS AND DISCUSSIONS

Continuous and regrown diodes

The SSPC spectrum of the continuously grown diode (sample 1) is presented in Fig. 3(a) and is very similar to that of *c*-plane *n*-GaN grown on the free-standing GaN.[24] Similar E_o values to those of Ref. 24 are adopted in this study; E_o = 1.9 eV, 2.9 eV, and 3.3 eV were determined for the deep level signature between 1.20 and 2.60 eV, 2.60 and 3.20 eV, and 3.30 and 3.45 eV, respectively. The origin of the E_c – 1.90 eV deep level is likely related to a native defect caused by atomic displacement during growth.[25] Defect levels near E_c – 2.9 eV in *n*-GaN are associated with either C[26] or Ga vacancy,[27] and it is likely that both defect sources are present in the film. The E_c – 3.3 eV defect state is likely the same as a level at E_c – 3.28 eV that is often ascribed to C impurities.[28] Previous reports on *m*-plane *n*-type GaN show a level at E_c – 3.31 eV, which was also attributed to C.[29]

Figure 3(b) indicates the depth profiling of the deep levels for sample 1 using the LCV method. Spatially uniform defect concentrations were observed for the as-grown *n*-type *m*-plane GaN, which is expected for a continuously grown film. The defect concentrations of the deep levels are similar to continuously grown *c*-plane oriented *n*-GaN on free-standing GaN substrates,[24] indicating that the concentration of point defects, and especially impurity-related defects, can be well controlled for epitaxial growth of *m*-plane GaN. The low defect density observed in the continuously grown sample corresponds well with the observed lowest reverse leakage characteristic in the *J*–*V* results (~4×10^{-5} A/cm^2 at −10 V) among all the samples tested in this study [Fig. 1(b)].

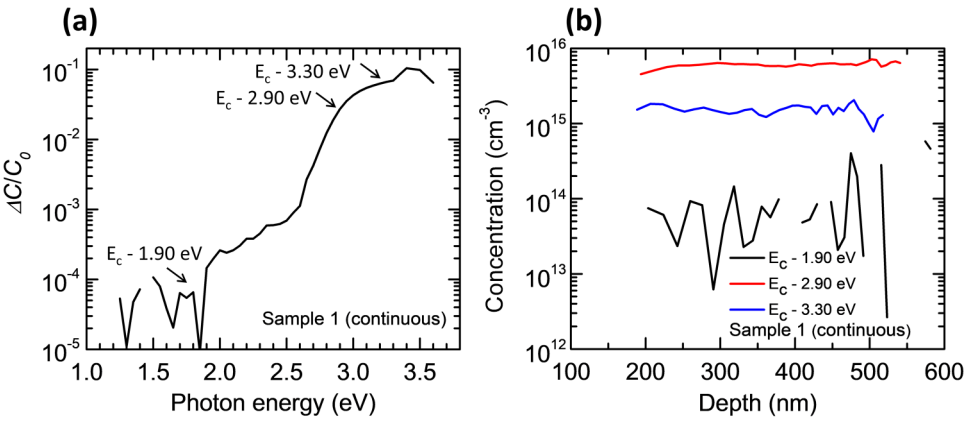

FIG. 3. (a) SSPC spectrum and (b) depth profile of the continuously grown Schottky diode (sample 1).

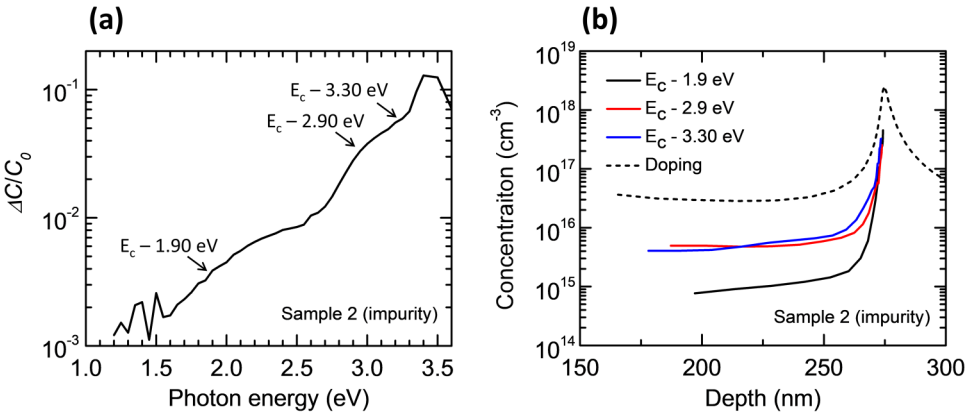

FIG. 4. (a) SSPC spectrum and (b) depth profile of the regrown impurity Schottky diode (sample 2).

A regrown Schottky diode (sample 2) was also studied to investigate the role of interfacial impurities and regrowth without any dry etching on defect levels in GaN. The SSPC spectrum is shown in Fig. 4(a) with the net doping profile measured by *C*–*V* and the defect concentration profile measured by LCV in Fig. 4(b). The SSPC spectrum in Fig. 4(a) was measured with a reverse voltage, $V_r = 0$ V, corresponding to a depletion region from 0 to 200 nm below the surface, i.e., 75 nm above the regrowth interface. The fill pulse (+0.5 V) was sufficient to reset the diode capacitance to near its dark value. The SSPC spectrum of the regrown diode [Fig. 4(a)] is qualitatively similar to that of the continuously grown diode [Fig. 3(a)], implying that the same type of deep level defects exists in both samples. However, the profile of these defect states in the regrown sample shows a strong depth dependence that is closely correlated to the regrowth interface. The doping profile shows a large spike at the depth of ∼275 nm from the sample surface [Fig. 4(b)], corresponding to the regrowth interface. The spike in the doping profile of the regrown sample was previously correlated with Si and/or O impurity spikes buried at the regrowth interface.[22] The peak N_t for all observed deep levels exceeds 10^{17} cm^{-3} just above the regrowth interface [Fig. 4(a)]. However, only ∼25 nm above the interface, N_t for the E_c – 2.9 and E_c – 3.30 eV defect levels reaches those of the as-grown continuously grown diode [Fig. 3(a)]. Considering prior impurity investigation of regrown *m*-plane GaN diodes indicating sharply peaked C concentration profiles at the regrowth interface, the observed trend here is also consistent with C related defects being the origin of the E_c – 2.9 eV and E_c – 3.3 eV levels.[22] The large-density of the E_c – 1.9 eV level (relative to the continuously grown sample) persists even over 75 nm above the regrowth interface, suggesting that elevated concentration of this defect level propagates to the upper layers during the regrowth process. A possible scenario is that the thermal desorption during the substrate ramp up (prior to initiating the epitaxial regrowth) generates some point defects at the regrowth interface, which may then diffuse to the upper layers.

A comparison of *J*–*V* data [Fig. 1(b)] between the continuously grown (sample 1) and the regrown (sample 2) diodes shows an ∼100× larger reverse *J* compared to that of the reference (sample 1), which is likely due to the increased concentration of the E_c – 1.9 eV deep levels. The E_c – 1.9 eV state is energetically located near midgap, which may give rise to efficient band-to-band tunneling and increase both forward and reverse leakage.[22,30] Furthermore, the gradually "saturated" forward current from sample 2 after 0.5 V may also be attributed to the increased interfacial impurities. One possible mechanism for such a behavior is an increased recombination at the regrowth junction. As the impurity spikes are highly localized to the regrowth interface, it may adversely affect the performance of regrown *p*–*n* diodes, especially if the regrowth interface is located right at the metallurgic junction, where the electric field is the highest.[22]

ICP etched-and-regrown diodes

Figure 5 presents the SSPC and LCV results of the baseline etched-and-regrown diode (sample 3). Similar to the regrown diode (sample 2), the etched-and-regrown diode (sample 3) also showed a spike in the doping at the regrowth interface. The depletion width was pinned at the regrowth interface, indicating an increase in N_D–N_A near the regrown interface. The Si doping level was the same for all the structures (∼6×10^{16} cm^{-3}), which suggests that the deep level defect concentration exceeds that of Si throughout the regrown region. Thus, ICP etching appeared to greatly increase the defect levels for the etched-and-regrown sample (sample 3) compared to just regrowth without ICP etching (sample 2). The SSPC spectrum for the ICP etched-and-regrown diode shows the same deep-level defect signatures as the continuously grown and regrown (without etch) diodes. However, the LCV data reveal a significantly increased level of defect density near the etched-and-regrown interface of sample 3 compared to the reference and regrown only samples (samples 1 and 2). Thus, defects associated with features from dry etching depend strongly on the depth away from the regrowth interface, which is also reported previously.[1–3] The peak concentrations of the E_c – 1.9 eV and E_c – 3.30 eV levels exceed 10^{18} cm^{-3} compared to ∼10^{17} cm^{-3} for the regrown diode. The defect concentration near the regrown surface could not be probed by LCV due to the fully depleted regrown drift region. However, the results from the regrown diode imply that the high concentration of the E_c – 1.9 eV relative to the nominal Si doping level persists well into the region above the regrowth interface. Dry etch subsurface damage has been previously shown to

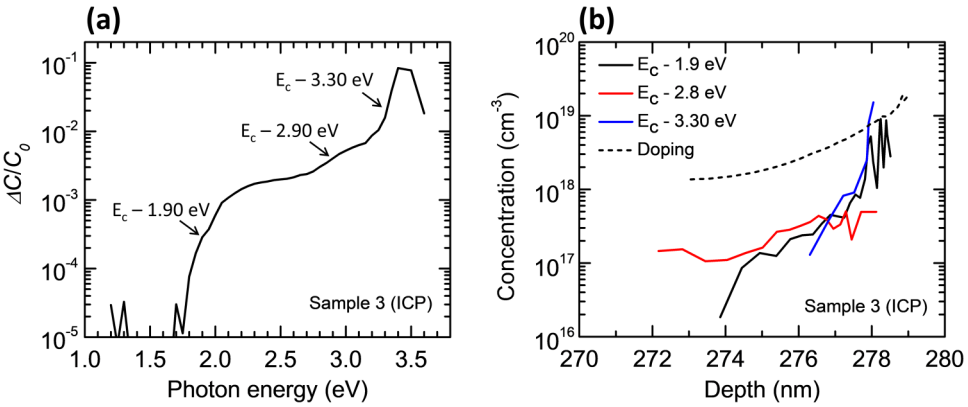

FIG. 5. (a) SPPC spectrum and (b) depth profile of the ICP etched-and-regrown Schottky-diode (sample 3).

extend several hundred angstroms (500–600 Å) below the surface, which is attributed to the creation of nitrogen vacancy-related shallow donors.[31–33] However, due to the increased charge interface at the regrown interface, the depletion region was not able to extend into the sub-surface region below the regrown interface for analysis. The effects of dry-etch and regrowth on the electrical performance of diodes have also been reported on c-plane GaN.[20,34,35] Increased leakage current in *p*–*n* diodes grown on the *c*-plane in both the forward and reverse bias has been correlated with dry etch-induced defects (E_c – 1.9 eV).[36] The origin of the E_c – 1.9 eV level is likely to be an intrinsic point defect, considering that it exists at a low concentration in a continuously grown material, has elevated concentration at a non-plasma etched regrowth interface (where thermal desorption may occur), and an even larger concentration at a plasma-etched regrowth interface, given that atomic displacement from ion bombardment is likely to occur during any plasma-based dry etching. The gallium interstitial (Ga_i) has been suggested as the source for the E_c – 1.9 eV deep level,[24] as its density increase coincides with the emergence of point defect clustering during proton irradiation of *c*-plane *n*-GaN. Also, due to the relatively high mobility of Ga_i at room temperature,[37] the point defect clustering may occur with a high probability considering Ga_i as the point defect. The impurity spike is large enough to provide net carriers throughout the regrown region for conductive diodes despite the elevated defect densities observed via LCV. Also, we believe that defects could diffuse far enough to travel from the etched layer into the regrown layer. However, diffusion does not need to occur to see an elevated defect density above the etched interface. Regrowth on a damaged "substrate" will produce defective materials for some time until the growth recovers to a nominal state, even if the substrate itself remains frozen in. The doping of the regrown layers is lightly doped *n*-type GaN (with N_D–N_A: $\sim 6 \times 10^{16}$ cm^{-3}). The charge observed in CV indicates an increase ($\sim 1.8 \times 10^{19}$ cm^{-3}) in N_D–N_A near the regrown interface. Previous reports have shown that p-type materials can become strongly compensated to high n-type 1×10^{19} cm^{-3} after exposure to a high density plasma.[38] Thus, the predominant impurity observed is shallow donors N_D which is confirmed by CV. A simple back of the envelop calculation was done to obtain a plasma ion flux considering Cl ions with the dimensions, pressure, voltages, and powers present during the etching of these samples. The plasma was found to have a flux of $\sim 1 \times 10^{15}$ cm^{-2} s^{-1}. With the surface density of GaN and time etched for these samples, it was found that a total of $\sim 1 \times 10^{19}$ atoms cm^{-3} will be influenced by the plasma. This calculation only assumes ion interactions, and chemical etching is also be present. In addition, stopping and range of ions in matter (SRIM) calculations also show a concentration of $\sim 3 \times 10^{18}$ cm^{-3} of displaced atoms. Even further consideration must be taken for the *m*-plane orientation studied. Nonpolar planes may be more susceptible to impurity incorporation than the *c*-plane due to the higher concentration of N atomic sites on nonpolar *m*-plane surfaces.[39–41] An additional percentage and N sites are available during etching which may lead to an increase in net donors N_D induced by ICP. Therefore, the increase in N_d carrier concentration observed is reasonable considering previous publications, calculations, and simulations. Electrical testing of sample 3 shows the highest reverse leakage of all samples. The interpretation of high defect density propagating to the surface is accompanied with ~1000× increase in reverse leakage of sample 3 compared to the reference (sample 1) [Fig. 1(b)].

The effect of a 10 min AZ400K at 80 °C treatment of the dry etched GaN material (sample 4) was also investigated to see whether the elevated defect levels could be mitigated near the regrowth interface. AZ400K is a KOH based solution that etches GaN very slowly[42] but could be sufficient to remove the surface defects. The results of SSPC [Fig. 6(a)] and LCV [Fig. 6(b)] of the ICP etched +AZ400K are shown. The same three defect levels as those for the other samples were observed in the SSPC spectrum. The peak N_t for all deep levels were drastically reduced for the ICP + AZ400K diode (sample 4) compared to the ICP baseline etched-and-regrown diode (sample 3) and were comparable to those for the regrown diode without ICP. The tail of the elevated defects from the regrowth interface into the bulk [Fig. 6(b)] was much longer for the ICP + AZ400K compared to the regrown without an etch sample. However, N_t for all deep levels reached the values observed in the reference continuously grown diode (sample 1). This is especially notable for the E_c – 1.9 eV deep level with a high N_t for the regrown sample (sample 2) compared to the reference (sample 1). This reduction in N_t for the E_c – 1.9 eV level explains the reduced reverse leakage for the ICP + AZ400K diode (sample 4) compared to the regrown diode without an etch (sample 2) [Fig. 1(b)].

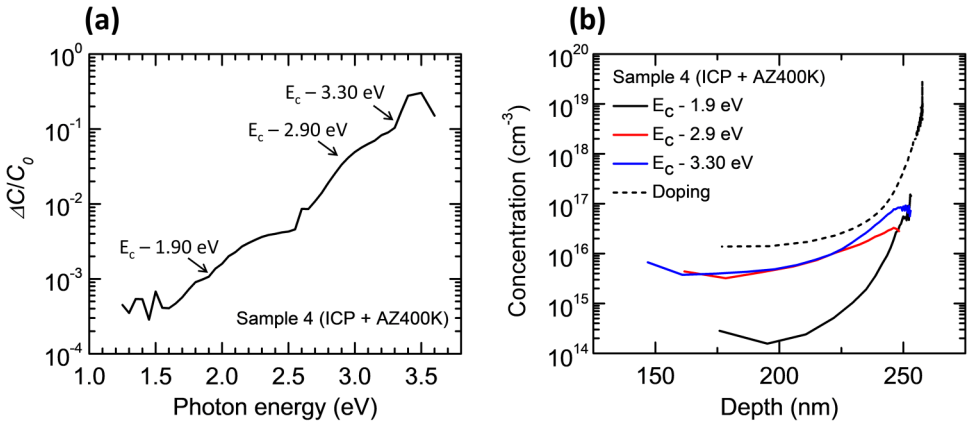

FIG. 6. (a) SSPC spectrum and (b) depth profile of the ICP + AZ400K etched-and-regrown Schottky-diode (sample 4).

ICP + PEC etched and regrown diodes

ICP etching is likely to generate sub-surface damage via ion bombardment which may not be readily removed with etchants with slow etch rates, such as AZ400K. While our results show that AZ400K is marginally effective in reducing defect levels associated with regrowth, additional methods for removing dry etch-induced damage should be investigated to reduce the defects further. PEC etching has previously been used to etch significant depths into GaN.[4,43–45] Therefore, it may be a suitable candidate for etching away damaged material caused by a dry etching process. For this purpose, the PEC etch rate was calibrated to approximately 2 nm/min of *n*-GaN (6×10^{16} cm^{-3}) using 0.01M KOH in de-ionized (DI) water at room temperature with a surface flux of 100 mW/cm^2.

The SSPC spectrum and depth profile of the ICP etched (200 nm deep) plus a subsequent PEC etching (400 nm deep) diode (sample 5) are presented in Fig. 7. The RMS roughness was measured after 400 nm of PEC etching using atomic force microscopy (AFM) to be ∼1.5 nm [Fig. 2(d)], which shows reduced roughness compared to an ICP etched only sample [Fig. 2(b)]. The same group of deep levels were observed in the ICP + PEC sample as in the other samples in this study [Fig. 7(a)]. No doping spike at the regrowth interface (∼500 nm depth) was observed [Fig. 7(b)] in the ICP + PEC sample (sample 5) using CV. However, the presence of Si ($\sim 5 \times 10^{17}$ cm^{-3}) and O ($\sim 6 \times 10^{17}$ cm^{-3}) "spikes" with a full width half max (FWHM) of ∼33 nm and ∼37 nm, respectively, is observed by secondary ion mass spectrometry (SIMS). The detection limits (sensitivity) of the analysis are Si = 3×10^{15} cm^{-3}, O = 1×10^{16} cm^{-3} with a depth resolution of 12.5 Å. It is unclear whether the lack of a doping spike in CV at the regrowth interface is a result of the PEC treatment or simply due to the sporadic nature of surface contamination by ambient exposure.[22,30] Interfacial impurities are likely to increase with ambient exposure and surface treatments. However, a lack of a doping spike (i.e., charge) does not necessarily indicate a lack of interfacial impurities as seen from the comparison of SIMS and CV. Therefore, the interfacial impurities are not completely ionized. A defect profile comparison of the ICP + AZ400K [Fig. 6(b)] and ICP + PEC [Fig. 7(b)] shows that the latter has a slightly lower N_t for the E_c – 1.9 eV level in the bulk but much lower (∼10^{16} cm^{-3}) N_t near the regrowth interface.

The decrease in the reverse leakage current of sample 5 (3×10^{-4} A/cm^2) as compared to the ICP etched only sample 3 (3×10^{-2} A/cm^2) is attributed to the removal of the dry-etch induced damage based on the reduction of all deep levels in sample

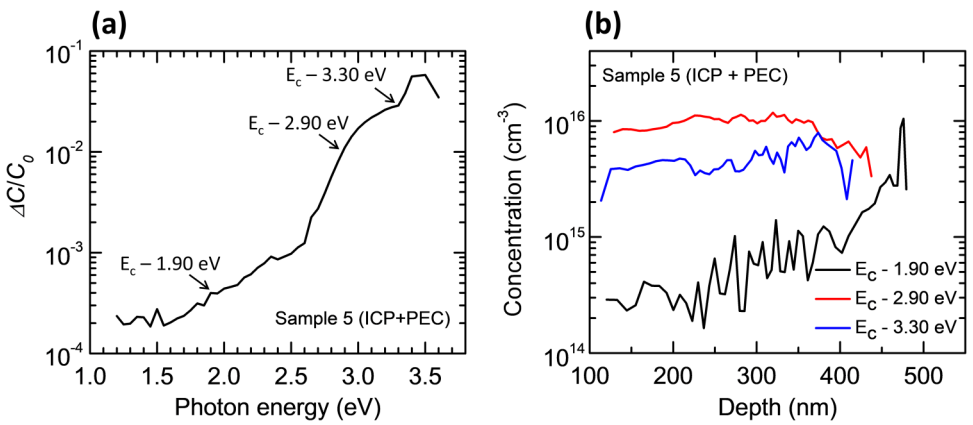

FIG. 7. (a) SSPC spectrum and (b) depth profile of the ICP + PEC etched-and-regrown Schottky diode (sample 5). The depth profile in (b) is taken near the regrowth interface.

6 compared to sample 3. Also, the E_c – 2.9 eV deep level is the highest N_t in the ICP + PEC diodes. Thus, the effect of this level is unlikely to contribute to the reverse leakage, as the ICP + PEC diodes coincide with the lowest reverse J compared to all other regrown samples (samples 2–4). This result is consistent with our previous report of a high-C interfacial layer which corresponds to the E_c – 2.9 eV deep level showing little effect on reverse leakage.[22]

Table I summarizes the deep-level defect densities for all the samples in this study near the regrown interface (close to the peak defect densities in the depth profile) and in the bulk region, where the defect density spectrum is flat away from the tail regions of the interface. The regrown sample (sample 2) did not show significant enhancement in any of the three deep levels (namely, E_c – 1.9 eV, E_c – 2.9 eV, and E_c – 3.3 eV) in the bulk region, while a localized enhancement in the deep levels near the regrowth interface was observed. The ICP etched-and-regrown sample, on the other hand, shows a significant enhancement of all the three deep levels in the bulk and near the regrowth interface. AZ400K (sample 4) and PEC (sample 5) treatments both significantly reduce the deep-level defect densities away from the regrown interface down to the levels close to those for the reference continuously grown sample (sample 1). The main difference between samples 4 and 5 is that localized defects near the regrowth interface were largely eliminated in the PEC treated sample (sample 5).

In addition, the ICP + PEC (sample 5) and the regrown without an etch (sample 2) samples have similar N_t for the E_c – 1.9 eV level in the regrown bulk, while the latter shows >10× higher leakage. Hence, the large spike in E_c –1.9 eV defect N_t ($>10^{17}$ cm^{-3}) for the regrown diode (and missing for the ICP + PEC sample), is likely to be the main contributor to leakage rather than background levels $N_t \sim 10^{15}$ cm^{-3} in the regrown bulk. The ICP + PEC sample also shows a lower N_t for the E_c – 1.9 eV level near the regrown interface even when compared to the regrown sample without a plasma etch, which may imply that the PEC not only removes etch-induced damage, but also may provide an epitaxial surface that is less susceptible to the formation of defects during the regrowth process. PEC may also be considered to replace the dry etch process to define the selective-area regrown region as it introduces significantly reduced levels as compared to ICP etching. However, PEC etching is not able to fully eliminate dry-etch-induced defect levels. Also, the concentration of the E_c – 2.9 eV level in the bulk is a bit higher, while the E_c – 3.3 eV concentration is almost the same in sample 5 compared to other samples. The wet treatment methods suggested in this work (both AZ400K and PEC) enable reduced damage, while maintaining smooth epitaxial-ready surfaces.

CONCLUSIONS

In summary, SSPC was performed on etched-and-regrown m-plane n-type Schottky diodes. As-grown levels were identified at E_c – 1.9 eV, E_c – 2.9 eV, and E_c – 3.3 eV with concentrations below $N_t \sim 10^{16}$ cm^{-3}. The origin of the E_c – 1.9 eV level is likely to be an intrinsic point defect introduced during growth where thermal desorption may occur. Defect levels near E_c – 2.9 eV are associated with either carbon or Ga vacancies, and the E_c – 3.3 eV defect state is likely ascribed to carbon impurities. In addition, localized levels associated with impurities and regrowth were observed for regrowth without an etch. However, by introducing an ICP etch process before regrowth a ∼100 000× increase in the E_c – 1.9 eV level with an emergent E_c – 3.3 eV level as compared to as-grown materials is observed near the regrowth surface. Thus, atomic displacement from ion bombardment is likely to occur during any plasma-based dry etching resulting in an even larger defect concentration at a plasma-etched regrowth interface. Depth profiling shows that the effect of these plasma-induced defects is not localized and may propagate several hundred nanometers away from the etched interface indicated by an observed tail for all defect levels. Further, JV testing confirms the effect of these elevated levels as leakage current was ∼1000× higher as compared to the as-grown material. Therefore, wet treatments were investigated to mitigate the elevated defect levels induced by dry etching. An AZ400K dip was introduced after ICP etching due to its ability to slowly etch GaN. The deep levels were significantly reduced near the regrown interface along with an ∼100× reduction in reverse leakage current compared to the ICP-etched only sample. An observed tail of the elevated defects from the regrowth interface into the bulk was again observed indicating only a partial mitigation of the etch-induced damage. Thus, a PEC wet-etch treatment after ICP-etching was investigated due to its ability to etch GaN at a higher rate than AZ400K. It was observed that the subsequent PEC treatment reduced the E_c – 1.9 eV level. Reverse leakage was also reduced by ∼1000× compared to the ICP-etched only sample. No observable tail in the depth profiling indicated that the deep levels induced by ICP etching did not propagate away from the regrowth interface in the ICP + PEC sample. Therefore, the wet treatment methods suggested in this work (both AZ400K and PEC) enable mitigation of ICP-etch induced damage on n-type m-plane GaN while maintaining smooth epitaxial-ready surfaces. Similar wet-etching methods have been implemented on the c-plane and are part of on-going investigation on etched-and-regrown c-plane diodes. By providing solutions to dry-etched induced damage using wet-treatments, the next generation of selective-doped high-power vertical electronics devices on GaN may be realized.

ACKNOWLEDGMENTS

The information, data, or work presented herein was funded in part by the Advanced Research Projects Agency—Energy (ARPA-E), U.S. Department of Energy (DOE) under the PNDIODES program directed by Dr. Isik Kizilyalli. Sandia National Laboratories is a multimission laboratory managed and operated by National Technology and Engineering Solutions of Sandia, LLC, a wholly owned subsidiary of Honeywell International, Inc., for the U.S. Department of Energy's National Nuclear Security Administration under Contract No. DE-NA-0003525. The views expressed in the article do not necessarily represent the views of the U.S. Department of Energy (DOE) or the United States Government.

DATA AVAILABILITY

The data that support the findings of this study are available from the corresponding author upon reasonable request.

REFERENCES

[1]J. G. Nedy, N. G. Young, K. M. Kelchner, Y. Hu, R. M. Farrell, S. Nakamura, S. P. DenBaars, C. Weisbuch, and J. S. Speck, Semicond. Sci. Technol. **30**, 085019 (2015).
[2]C.-Y. Fang, W.-J. Huang, E. Y. Chang, C.-F. Lin, and M.-S. Feng, Jpn. J. Appl. Phys. **42**, 4207–4212 (2003).
[3]X. A. Cao, S. J. Pearton, G. T. Dang, A. P. Zhang, F. Ren, and J. M. Van Hove, IEEE Trans. Electron Devices **47**, 1320–1324 (2000).
[4]V. Meyers, E. Rocco, K. Hogan, S. Tozier, B. McEwen, I. Mahaboob, and F. Shahedipour-Sandvik, J. Electron. Mater. **49**, 3481–3489 (2020).
[5]E. A. Jones, F. F. Wang, and D. Costinett, IEEE J. Emerg. Sel. Topics Power Electron. **4**, 707–719 (2016).
[6]J. Y. Tsao, S. Chowdhury, M. A. Hollis, D. Jena, N. M. Johnson, K. A. Jones, R. J. Kaplar, S. Rajan, C. G. Van de Walle, E. Bellotti, C. L. Chua, R. Collazo, M. E. Coltrin, J. A. Cooper, K. R. Evans, S. Graham, T. A. Grotjohn, E. R. Heller, M. Higashiwaki, M. S. Islam, P. W. Juodawlkis, M. A. Khan, A. D. Koehler, J. H. Leach, U. K. Mishra, R. J. Nemanich, R. C. N. Pilawa-Podgurski, J. B. Shealy, Z. Sitar, M. J. Tadjer, A. F. Witulski, M. Wraback, and J. A. Simmons, Adv. Electron. Mater. **4**, 1600501 (2018).
[7]T. J. Flack, B. N. Pushpakaran, and S. B. Bayne, J. Electron. Mater. **45**, 2673–2682 (2016).
[8]J. A. Edmond and R. F. Davis, U.S. patent 50,875,76A (11 February 1992).
[9]Y. Zhang, Z. Liu, M. J. Tadjer, M. Sun, D. Piedra, C. Hatem, T. J. Anderson, L. E. Luna, A. Nath, A. D. Koehler, H. Okumura, J. Hu, X. Zhang, X. Gao, B. N. Feigelson, K. D. Hobart, and T. Palacios, IEEE Electron Device Lett. **38**, 1097–1100 (2017).
[10]D. Ji and S. Chowdhury, IEEE Trans. Electron Devices **62**, 2571–2578 (2015).
[11]D. Ji, Y. Yue, J. Gao, and S. Chowdhury, IEEE Trans. Electron Devices **63**, 4011–4017 (2016).
[12]J. R. Dickerson, A. A. Allerman, B. N. Bryant, A. J. Fischer, M. P. King, M. W. Moseley, A. M. Armstrong, R. J. Kaplar, I. C. Kizilyalli, O. Aktas, and J. J. Wierer, IEEE Trans. Electron Devices **63**, 419–425 (2016).
[13]J. Du, Z. Li, D. Liu, Z. Bai, Y. Liu, and Q. Yu, Superlatt. Microstruct. **111**, 302–309 (2017).
[14]I. C. Kizilyalli, A. P. Edwards, O. Aktas, T. Prunty, and D. Bour, IEEE Trans. Electron Devices **62**, 414–422 (2015).
[15]I. C. Kizilyalli, A. P. Edwards, H. Nie, P. Bui-Quang, D. Disney, and D. Bour, IEEE Electron Device Lett. **35**, 654–656 (2014).
[16]T. Oka, T. Ina, Y. Ueno, and J. Nishii, Appl. Phys. Express **8**, 054101 (2015).
[17]H. Nie, Q. Diduck, B. Alvarez, A. P. Edwards, B. M. Kayes, M. Zhang, G. Ye, T. Prunty, D. Bour, and I. C. Kizilyalli, IEEE Electron Device Lett. **35**, 939–941 (2014).
[18]S. Chowdhury, B. L. Swenson, M. H. Wong, and U. K. Mishra, Semicond. Sci. Technol. **28**, 074014 (2013).
[19]S. R. Alugubelli, H. Fu, K. Fu, H. Liu, Y. Zhao, M. R. McCartney, and F. A. Ponce, Appl. Phys. Lett. **115**, 201602 (2019).
[20]K. Fu, H. Fu, X. Huang, H. Chen, T.-H. Yang, J. Montes, C. Yang, J. Zhou, and Y. Zhao, IEEE Electron Device Lett. **40**, 1728–1731 (2019).
[21]R. M. Farrell, D. A. Haeger, X. Chen, M. Iza, A. Hirai, K. M. Kelchner, K. Fujito, A. Chakraborty, S. Keller, S. P. DenBaars, J. S. Speck, and S. Nakamura, J. Cryst. Growth **313**, 1–7 (2010).
[22]A. Aragon, M. Monavarian, I. Stricklin, G. Pickrell, M. Crawford, A. Allerman, A. M. Armstrong, and D. Feezell, Phys. Status Solidi A **1900757**, 1–7 (2019).
[23]A. Armstrong, A. R. Arehart, and S. A. Ringel, J. Appl. Phys. **97**, 083529 (2005).
[24]K. C. Collins, A. M. Armstrong, A. A. Allerman, G. Vizkelethy, S. B. Van Deusen, F. Léonard, and A. A. Talin, J. Appl. Phys. **122**, 235705 (2017).
[25]S. Limpijumnong and C. Van de Walle, Phys. Rev. B **69**, 035207 (2004).
[26]T. Ogino and M. Aoki, Jpn. J. Appl. Phys. **19**, 2395 (1980).
[27]A. Hierro, S. A. Ringel, M. Hansen, J. S. Speck, U. K. Mishra, and S. P. DenBaars, Appl. Phys. Lett. **77**, 1499–1501 (2000).
[28]A. Armstrong, A. R. Arehart, D. Green, U. K. Mishra, J. S. Speck, and S. A. Ringel, J. Appl. Phys. **98**, 053704 (2005).
[29]T. A. Henry, A. Armstrong, K. M. Kelchner, S. Nakamura, S. P. DenBaars, and J. S. Speck, Appl. Phys. Lett. **100**, 082103 (2012).
[30]M. Monavarian, G. Pickrell, A. A. Aragon, I. Stricklin, M. H. Crawford, A. A. Allerman, K. C. Celio, F. Léonard, A. A. Talin, A. M. Armstrong, and D. Feezell, IEEE Electron Device Lett. **40**, 387–390 (2019).
[31]X. A. Cao, H. Cho, S. J. Pearton, G. T. Dang, A. P. Zhang, F. Ren, R. J. Shul, L. Zhang, R. Hickman, and J. M. Van Hove, Appl. Phys. Lett. **75**, 232–234 (1999).
[32]K. J. Choi, H. W. Jang, and J.-L. Lee, Appl. Phys. Lett. **82**, 1233–1235 (2003).
[33]X. A. Cao, A. P. Zhang, G. T. Dang, F. Ren, S. J. Pearton, R. J. Shul, and L. Zhang, J. Vac. Sci. Technol. A **18**, 1144–1148 (2000).
[34]K. Fu, H. Fu, X. Huang, T.-H. Yang, C.-Y. Cheng, P. R. Peri, H. Chen, J. Montes, C. Yang, J. Zhou, X. Deng, X. Qi, D. J. Smith, S. M. Goodnick, and Y. Zhao, IEEE J. Electron Devices Soc. **8**, 74–83 (2020).
[35]K. Fu, H. Fu, H. Liu, S. R. Alugubelli, T.-H. Yang, X. Huang, H. Chen, I. Baranowski, J. Montes, F. A. Ponce, and Y. Zhao, Appl. Phys. Lett. **113**, 233502 (2018).
[36]G. W. Pickrell, A. M. Armstrong, A. A. Allerman, M. H. Crawford, C. E. Glaser, J. Kempisty, and V. M. Abate, J. Appl. Phys. **126**, 145703 (2019).
[37]K. H. Chow, G. D. Watkins, A. Usui, and M. Mizuta, Phys. Rev. Lett. **85**, 2761–2764 (2000).
[38]X. A. Cao, S. J. Pearton, A. P. Zhang, G. T. Dang, F. Ren, R. J. Shul, L. Zhang, R. Hickman, and J. M. Van Hove, Appl. Phys. Lett. **75**, 2569–2571 (1999).
[39]N. A. Fichtenbaum, T. E. Mates, S. Keller, S. P. DenBaars, and U. K. Mishra, J. Cryst. Growth **310**, 1124–1131 (2008).
[40]S. C. Cruz, S. Keller, T. E. Mates, U. K. Mishra, and S. P. DenBaars, J. Cryst. Growth **311**, 3817–3823 (2009).
[41]D. A. Browne, E. C. Young, J. R. Lang, C. A. Hurni, and J. S. Speck, J. Vac. Sci. Technol. A **30**, 041513 (2012).
[42]D. Zhuang and J. H. Edgar, Mater. Sci. Eng. R Rep. **48**, 1–46 (2005).
[43]M. S. Minsky, M. White, and E. L. Hu, Appl. Phys. Lett. **68**, 1531–1533 (1996).
[44]C. O. Holder, J. T. Leonard, R. M. Farrell, D. A. Cohen, B. Yonkee, J. S. Speck, S. P. DenBaars, S. Nakamura, and D. F. Feezell, Appl. Phys. Lett. **105**, 031111 (2014).
[45]Y. Gao, M. D. Craven, J. S. Speck, S. P. Den Baars, and E. L. Hu, Appl. Phys. Lett. **84**, 3322–3324 (2004).